Quantum phase diagram of Shiba impurities from bosonization

Tomás Bortolin,[1,2,*] Aníbal Iucci,[1,2,†] and Alejandro M. Lobos[3,‡]
[1]*Instituto de Física La Plata - CONICET, Diag 113 y 64 (1900) La Plata, Argentina*
[2]*Departamento de Física, Universidad Nacional de La Plata, cc 67, 1900 La Plata, Argentina*
[3]*Facultad de Ciencias Exactas y Naturales, Universidad Nacional de Cuyo and CONICET, 5500 Mendoza, Argentina*

(Received 12 May 2019; revised manuscript received 17 August 2019; published 7 October 2019)

A characteristic feature of magnetic impurities in superconductors is the existence of a spin- and parity-changing quantum phase transition (known as "0-π" transition) which has been observed in scanning tunneling microscopy (STM) and quantum transport experiments. Using the Abelian bosonization technique, here we analyze the ground-state properties and the quantum phase diagram of an artificial "Shiba impurity" in a one-dimensional superconductor. Within the bosonization framework, the ground-state properties are determined by simple solitonlike solutions of the classical equations of motion of the bosonic fields, whose topological charge is related to the spin and fermion-parity quantum numbers. Interestingly, the same theoretical framework can be used in the case of a bulk superconductor, where previous results can be rederived in an elegant fashion. Our results indicate that the quantum phase diagram of a magnetic impurity in the superconductor can be strongly affected by geometrical and dimensional effects. Exploiting this fact, in the one-dimensional case we propose an experimental superconducting setup in which a novel parity-preserving, spin-changing "0-0" transition is predicted.

DOI: 10.1103/PhysRevB.100.155111

I. INTRODUCTION

Yu-Shiba-Rusinov (or simply Shiba) states are localized subgap states arising in a superconductor due to the local pair-breaking processes induced by a magnetic impurity [1–4] or by a quantum dot in superconductor-hybrid nanodevices, where they are more commonly known as "Andreev bound states" [5–8]. Recently, these systems have become the focus of intensive research due to the prediction that Majorana zero modes (i.e., non-Abelian quasiparticles with potential uses in fault-tolerant topological quantum computation [9]) could be realized in a linear chain of magnetic impurities deposited on top of a superconductor. In these systems, the Shiba states can overlap along the chain forming a topological "Shiba band" [10–13], which at low temperatures mimics the physics of the Kitaev one-dimensional model [14]. Subsequent STM studies of chains of Fe atoms deposited on top of clean Pb surfaces have shown compelling evidence for the Majorana scenario [15–18], generating a lot of excitement.

A salient feature of Shiba systems is the existence of an experimentally accessible quantum phase transition, known as the "0-π transition," determined by the position of the level inside the superconducting gap: If the Shiba state falls below the Fermi energy, it becomes occupied and the nature of the collective ground state changes from an even-parity BCS-like singlet to an odd-parity spin-1/2 doublet [19]. This parity- and spin-changing transition has been experimentally observed both in adatom/superconductor systems with STM techniques [20,21] and in superconductor-quantum dot devices via quantum transport experiments [6,8,22–24].

Recent progress in nanofabrication has allowed the realization of ultrathin superconducting epitaxial nanostructures [i.e., one-dimensional nanowires (1DNWs)] using the proximity effect, where a "hard" superconducting gap has been induced [25,26]. These advances pave the way for novel technological applications and can potentially enable the study of Shiba states in systems with reduced dimensionality. A question which naturally arises in this context is whether the different dimensionality or geometrical properties of the superconductor can modify the properties of Shiba systems and the above-mentioned phase transition. For instance, scattering processes which are crucial in the one-dimensional (1D) geometry can be profoundly affected by interactions [27,28] or interference effects. In a 1D system (such as a proximitized 1DNW), the enhanced effect of correlations might indeed change the properties of a superconductor, thus modifying the features of the induced quantum phases.

In this work we implement the Abelian bosonization formalism to study the zero-temperature phase diagram of a Shiba impurity, both in a 1D and in a three-dimensional (3D) superconductor. Interestingly, within the bosonic representation the ground-state properties in both geometries can be studied in a unified way. In particular for the 1D case, we propose an experimental device based on proximitized semiconducting 1DNWs with a nearby ferromagnetic insulator nanowire grown on top (see Fig. 1) to induce a controllable Shiba state. We predict that this device could host a novel fermion parity-conserving, spin-changing "0-0" transition. Our results might have an impact in recent theoretical and experimental developments where Shiba states have been observed and in recent works where superconductivity is

*bortolin@fisica.unlp.edu.ar
†iucci@fisica.unlp.edu.ar
‡alejandro.martin.lobos@gmail.com

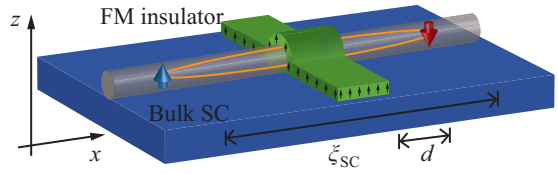

FIG. 1. Side view of the 1D semiconductor nanowire (in gray) proximitized by a bulk superconductor (blue region). An "artificial" magnetic impurity can be generated in this setup depositing a perpendicular ferromagnetic insulator (FMI) nanowire of width d much smaller than the coherence length ξ_{1D}.

induced in semiconducting nanowires by means of proximity effect.

II. THEORETICAL MODEL IN 1D

We describe a proximitized single-channel superconducting 1DNW of length $2L_W$ with the Hamiltonian $H = H_0 + H_\Delta + H_M^{1D}$, where

$$H_0 = \int_{-L_W}^{L_W} dx \left[\sum_\sigma \Psi_\sigma^\dagger \left(-\frac{\partial_x^2}{2m} \right) \Psi_\sigma + U \Psi_\uparrow^\dagger \Psi_\uparrow \Psi_\downarrow^\dagger \Psi_\downarrow \right] \quad (1)$$

describes the "normal" part of the interacting wire. Here, $\Psi_\sigma = \Psi_\sigma(x)$ annihilates a fermion with spin $\sigma = \uparrow, \downarrow$, and $U > 0$ is a repulsive Hubbard-type interaction parameter (here we have used $\hbar = 1$). For later convenience, we assume a closed wire with periodic boundary conditions

$$\Psi_\sigma(x) = \Psi_\sigma(x + 2L_W), \quad (2)$$

and then we take the limit $L_W \to \infty$. Linearization of the 1DNW spectrum in a region of width 2Λ around the Fermi energy allows us to write the Fermi fields as $\Psi_\sigma(x) = e^{ik_F x}\psi_{L\sigma}(x) + e^{-ik_F x}\psi_{R\sigma}(x)$, where k_F is the Fermi wave vector, and $\psi_{r\sigma}(x)$ with $r = L(R)$ are left- (right-)moving chiral fields slowly varying on the scale k_F^{-1}. We now introduce the bosonization formalism [29,30] and represent the chiral fermion fields as

$$\psi_{r\sigma}(x) = \frac{F_{r\sigma}}{\sqrt{2\pi a}} e^{-ir\phi_{r\sigma}(x)}, \quad (3)$$

where $\phi_{r\sigma}(x)$ are chiral bosonic fields obeying the Kac-Moody commutation relations $[\phi_{r\sigma}(x), \phi_{r'\sigma'}(x')] = i\pi r \delta_{r,r'}, \delta_{\sigma,\sigma'} \mathrm{sgn}(x - x')$, $a \sim k_F^{-1}$ is the short-distance cutoff of the continuum theory, and $F_{r\sigma}$ are standard Klein factors which ensure the proper anticommutation relations of the Fermi fields.

To simplify the physical interpretation of these bosonic fields, it is customary to introduce the transformation

$$\phi_{r\sigma} = \tfrac{1}{2}[\phi_c + r\theta_c + \sigma(\phi_s + r\theta_s)], \quad (4)$$

which satisfies canonical commutation relations $[\phi_\mu(x), \partial_y \theta_\nu(y)] = -2i\pi\delta_{\mu\nu}\delta(x - y)$ and where $c(s)$ refers to charge- (spin-)type operators. Here the convention $r = +1(-1)$ on the r.h.s has been used for the $R(L)$ branch, and similarly, $\sigma = +1(-1)$ for $\uparrow$ ($\downarrow$). Physically, the field $\phi_s(x)$ is related to the spin density operator

$$\begin{aligned} \rho_s(x) &= \frac{\Psi_\uparrow^\dagger \Psi_\uparrow - \Psi_\downarrow^\dagger \Psi_\downarrow}{2} \\ &= -\frac{\partial_x \phi_s}{2\pi} + \frac{1}{4\pi a}[e^{i2k_F x} e^{i\phi_c}(e^{i\phi_s} F_{R\uparrow}^\dagger F_{L\uparrow} \\ &\quad - e^{-i\phi_s} F_{R\downarrow}^\dagger F_{L\downarrow}) + \mathrm{H.c.}], \end{aligned} \quad (5)$$

while the field $\theta_c(x)$ is the Josephson phase field of the 1D superconductor, related to the charge-current density through the relation $j(x) = -2ev_c K_c \partial_x \theta_c(x)/\pi$. In terms of these fields, the Hamiltonian H_0 takes a Luttinger liquid form with decoupled charge and spin bosonic sectors, i.e., $H_0 = H_c + H_s$, where (see Refs. [29,30] for details)

$$H_\nu = \frac{v_\nu}{4\pi} \int_{-L_W}^{L_W} dx \left[\frac{1}{K_\nu} (\partial_x \phi_\nu)^2 + K_\nu (\partial_x \theta_\nu)^2 \right], \quad (6)$$

for $\nu = c, s$. The parameter K_ν encodes the interactions in each sector [i.e., $K_\nu < 1 (K_\nu > 1)$ corresponds to repulsive(attractive) interactions] and physically controls the decay of the correlation function $\langle \Psi_{r\sigma}(x) \Psi_{r\sigma}^\dagger(x') \rangle \sim |x - x'|^{-(K_c + K_s)}$. In our particular case, $K_c = 1/\sqrt{1 + Ua/(\pi v_F)}$, and due to the SU(2) symmetry of the model, the value of K_s should be constrained to $K_s = 1$. On the other hand, $v_c = v_F \sqrt{1 + Ua/(\pi v_F)}$ is the velocity of the 1D charge plasmons, and v_s is the velocity of the 1D spinons [29,30]. However, for generality purposes, in what follows we will assume a more generic situation where both K_s and v_s can take different values due to, e.g., the unaccounted presence of SU(2) symmetry-breaking terms, and whenever we need to make contact with our specific model, we will set $K_s = 1$ and $v_s = v_F$.

Proximity-induced superconductivity in the 1DNW is described by the term [31–33]

$$\begin{aligned} H_\Delta^{1D} &= \Delta \int_{-L_W}^{L_W} dx \, [\Psi_\uparrow^\dagger \Psi_\downarrow^\dagger + \mathrm{H.c.}] \\ &= \Delta \int_{-L_W}^{L_W} dx \, [\psi_{L\uparrow}^\dagger \psi_{R\downarrow}^\dagger + \psi_{R\uparrow}^\dagger \psi_{L\downarrow}^\dagger + \mathrm{H.c.}], \end{aligned} \quad (7)$$

where we have neglected the rapidly oscillating terms proportional to $e^{\pm i2k_F x}$ since they average to zero. Physically, the induced pairing potential Δ emerges from the integration of the bulk superconductor and strongly depends on the transparency and disorder of the superconductor/nanowire contact [25,26,34]. In terms of the bosonic fields, the pairing term writes

$$H_\Delta^{1D} = \frac{2\Delta}{\pi a} \int_{-L_W}^{L_W} dx \, \cos\theta_c(x) \cos\phi_s(x). \quad (8)$$

A simple scaling analysis where we rescale the cutoff $a \to a(1 + d\ell)$ indicates that H_Δ^{1D} is a relevant perturbation in the RG sense, i.e., $d\Delta(\ell)/d\ell = (2 - 1/K_c)\Delta(\ell)$, and flows to strong coupling as $\ell \to \infty$ when $K_c > 1/2$ [35,36].

We now introduce the effect of a classical magnetic impurity in the 1DNW. Although this is a well-known problem studied originally in Refs. [1–3] for the case of a classical spin in a noninteracting bulk BCS superconductor, here we focus on an *interacting* system in a one-dimensional geometry, and

therefore we expect important differences with respect to the original works by Yu, Shiba, and Rusinov.

In order to connect our work with concrete experimental realizations, in what follows we assume that the effect of a classical spin in the 1DNW can be *mimicked* by the exchange field generated by a nearby ferromagnetic-insulator (FMI) nanowire, grown perpendicularly to the 1DNW [32,37,38] (see Fig. 1). We assume that the width d of the FMI nanowire is much smaller than ξ_{1D}, the coherence length in the 1DNW. Under such circumstances, for all practical purposes the local exchange field becomes a pointlike perturbation (i.e., an artificial "magnetic impurity") from the perspective of the chiral fields $\psi_{r\sigma}(x)$. In contrast to real magnetic impurities (i.e., atoms of Co, Fe, Mn, etc., in the semiconducting nanowire) whose position and amount is unknown/uncontrolled for a particular experimental realization, the proposed device would have the advantage that induced subgap states could be controlled *in situ* by changing the magnetization of the FMI by, e.g., spin currents or external magnetic fields. Therefore, we assume the following Hamiltonian

$$H_M^{1D} = V \int_{-L_W}^{L_W} dx\, m_z(x)\rho_s(x), \tag{9}$$

where V is the average exchange field of the FMI nanowire, and $m_z(x)$ is its dimensionless magnetization (assumed to be oriented along the z axis) of the magnetic insulator which takes values between $-1 \leqslant m_z(x) \leqslant 1$. For concreteness, here we assume a Gaussian magnetic profile $m_z(x) = m_0 \exp(-x^2/d^2)$, where $m_0 = \pm 1$. Therefore, under the reasonable assumption that $k_F^{-1} \ll d \ll \xi_{1D}$, the magnetization of the STM tip can be approximated by $m_z(x) \sim m_0 d\sqrt{\pi}\delta(x)$.

Note that the assumption $k_F^{-1} \ll d$ allows us to further simply our model, since in that case single-particle backscattering processes (i.e., scattering processes with momentum transfer $\Delta q \simeq 2k_F$ between the R and L branches) can be ignored. This fact allows us to neglect all rapidly oscillating terms proportional to $\sim e^{\pm i2k_F x}$ in Eq. (5), since they average to zero. Note that this fact makes the proposed device very different from the usual superconductor-quantum dot hybrid devices [5–8], where backscattering processes are unavoidable and appear in the form of a non-negligible reflection coefficient from the quantum dot. Then, in the absence of single-particle backscattering terms, the spin density operator Eq. (5) can be approximated as $\rho_s(x) \simeq -\partial_x\phi_s(x)/2\pi$, and therefore the bosonized Hamiltonian can be written as

$$H_M^{1D} = -2\frac{v_s\delta_0}{K_s}\frac{\partial_x\phi_s(0)}{\pi}, \tag{10}$$

where we have defined the phase shift due to the scattering with the localized exchange-field potential as [39]

$$\delta_0 = \arctan\left(\frac{V m_0 d\sqrt{\pi}K_s}{4v_s}\right). \tag{11}$$

We note that in the absence of BCS pairing, the Hamiltonian $H_0 + H_M^{1D}$ is akin to the x-ray edge problem [29,30].

Interestingly, within the bosonization framework the total spin along the z axis s_z and fermion parity of the ground state $P = (-1)^J$ can be obtained from simple expressions in terms of the bosonic fields:

$$s_z = -\int_{-L_W}^{L_W} dx\, \frac{\partial_x\phi_s(x)}{2\pi} = -\frac{\Delta\phi_s}{2\pi}, \tag{12}$$

$$J = \int_{-L_W}^{L_W} dx\, \frac{\partial_x\theta_c(x)}{\pi} = \frac{\Delta\theta_c}{\pi}. \tag{13}$$

Due to the original periodic boundary conditions [see Eq. (2)], the following boundary conditions hold for the bosonic fields

$$\phi_{r\sigma}(x + 2L_W) = \phi_{r\sigma}(x) + 2\pi n_{r\sigma}, \tag{14}$$

with $n_{r\sigma}$ integer numbers. From here, it is easy to show that $2s_z$ and J are *topological* quantum numbers fully characterizing the ground state of the 1DNW. The relationship of J with the fermion parity of the ground state can be understood noting that the periodic boundary conditions impose $J + N \bmod 2 = 0$, with N the total number of particles in the 1DNW (see Ref. [40]). Since the fermion parity is defined as $P = (-1)^N$, from the previous relations we obtain $P = (-1)^J$. This is consistent with the fact that, although N is not a good quantum number, the pairing Hamiltonian Eq. (7) preserves the fermionic parity.

III. CLASSICAL EQUATIONS OF MOTION

We now focus on the ground-state properties of the system when the parameter Δ flows to strong coupling and becomes the dominant energy scale [i.e., when it becomes of the order of the ultraviolet cutoff $\Delta(\ell^*) \simeq \Lambda$]. To that end, we note that the Hamiltonian H_Δ^{1D} only couples the commuting fields $\phi_s(x)$ and $\theta_c(x)$, and therefore it is easy to see that both fields can be *simultaneously* chosen to minimize the energy. This fact allows us to obtain a well-defined classical limit, from where useful information about the strongly-correlated ground state can be extracted.

We now proceed to obtain classical equations of motion of the system. To that end, we define the canonically conjugated momenta of the fields $\phi_s(x)$ and $\theta_c(x)$, as $\Pi_s(x) = \frac{1}{\pi}\partial_x\theta_s(x)$ and $\Pi_c(x) = \frac{1}{\pi}\partial_x\phi_c(x)$, respectively. The Lagrangian density of the system is therefore expressed as

$$\mathcal{L}(x) = \Pi_s(x)\partial_t\phi_s(x) + \Pi_c(x)\partial_t\theta_c(x) - \mathcal{H}(x), \tag{15}$$

where

$$\begin{aligned}\mathcal{H}(x) = {} & \frac{v_c}{4\pi}\left[\frac{1}{K_c}(\pi\Pi_c(x))^2 + K_c(\partial_x\theta_c(x))^2\right] \\ & + \frac{v_s}{4\pi}\left[K_s(\pi\Pi_s(x))^2 + \frac{1}{K_s}(\partial_x\phi_s(x) - 4\delta_0\delta(x))^2\right] \\ & + \frac{2\Delta}{\pi a}\cos\theta_c(x)\cos\phi_s(x)\end{aligned} \tag{16}$$

is the Hamiltonian density of the 1DNW, obtained directly from Eqs. (6), (8), and (10), and where we have neglected a constant (and formally divergent) contribution independent of the fields. The classical equations of motion for the fields $\theta_c(x)$ and $\phi_s(x)$ are given by the Euler-Lagrange equations

$\partial_\mu \frac{\partial \mathcal{L}}{\partial(\partial_\mu \varphi)} = \frac{\partial \mathcal{L}}{\partial \varphi}$, which in the static case yield

$$\partial_x^2 \phi_s(x) = -\frac{g}{1-\zeta} \cos\theta_c(x) \sin\phi_s(x) + 4\delta_0 \delta'(x), \tag{17}$$

$$\partial_x^2 \theta_c(x) = -\frac{g}{1+\zeta} \sin\theta_c(x) \cos\phi_s(x), \tag{18}$$

where we have introduced the parameter $g \equiv 8\Delta/[a(v_c K_c + v_s/K_s)]$, related to the superconducting coherence length through the relation $\xi_{1D} = g^{-1/2}$. Note that the interactions in the 1DNW *can also affect* the coherence length through the dependence on the Luttinger parameters K_c and K_s. Finally, the "helicity" parameter

$$\zeta = \frac{v_c K_c - v_s/K_s}{v_c K_c + v_s/K_s} \tag{19}$$

measures the relative stiffness of the $\theta_c(x)$ field versus the stiffness of $\phi_s(x)$. For $\zeta < 0$, the deformations of $\theta_c(x)$ are energetically more expensive than those of $\phi_s(x)$, and vice versa for $\zeta > 0$. Finally, $\delta'(x)$ is the derivative of the Dirac delta function, which has to be interpreted in terms of the approximant $\delta(x) = \lim_{a\to 0} f(x,a)$ as $\delta'(x) = \lim_{a\to 0} \partial_x f(x,a)$.

Physically, Eqs. (17) and (18) determine the ground-state configurations of the fields $\phi_s(x)$ and $\theta_c(x)$. Note that the effect of the impurity potential Eq. (10) is *fully encoded* in the $4\delta_0\delta'(x)$ term, which introduces an inhomogeneity in the $\phi_s(x)$ field at the origin. The classical energy of these static solutions is obtained by replacing them directly into the classical Hamiltonian density $\mathcal{H}_{cl}(x)$, which follows from $\mathcal{H}(x)$ after setting the canonically-conjugated momenta to zero, i.e. $\Pi_s(x) = \Pi_c(x) = 0$. Then, the expression of the classical ground state energy is

$$E = \int_{-L_W}^{L_W} dx\, \mathcal{H}_{cl}(x). \tag{20}$$

Unfortunately, Eqs. (17) and (18) do not have a generic analytical solution. In order to gain physical insight, in the following sections we explore different cases, where simple or approximate analytical solutions can be found: (A) Absence of impurity, (B) helical point $\zeta = 0$, and (C) approximate results for finite ζ.

IV. RESULTS

A. Absence of impurity (case $\delta_0 = 0$)

As a pedagogical preparation to understand the more involved case of a classical impurity in a superconductor, it is instructive to analyze first the clean (albeit interacting) superconducting 1DNW. In the absence of the magnetic impurity, the last term in Eq. (17) vanishes, and the most relevant solutions at low energies are:

(1) The uniform and topologically-trivial solutions:

$$\left(\phi_s^{(0)}, \theta_c^{(0)}\right) = (\pi m, \pi n), \tag{21}$$

where (m, n) are integer numbers (even,odd) or (odd, even). These uniform solutions minimize the pairing term $H_\Delta^{1D} \sim \Delta \cos\phi_s^{(0)} \cos\theta_c^{(0)}$ in Eq. (8) and physically represent the "classical" BCS ground state (i.e., the filled Fermi sea of Bogoliubov quasiparticles). Evaluating the net z component of the spin and the fermion-parity index J of these configurations from Eqs. (12) and (13), respectively, yields

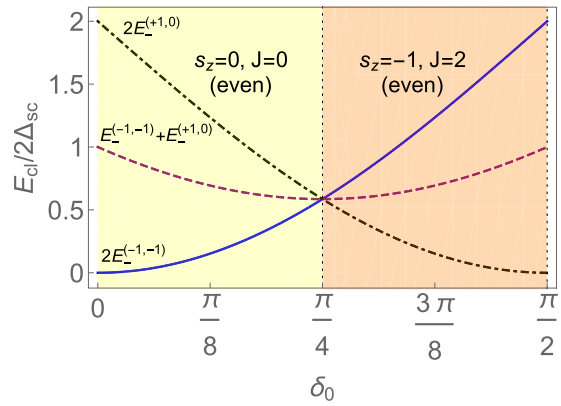

FIG. 2. Quantum phase diagram and lowest energy branches as functions of the phase shift δ_0 of the 1DNW system at the helical point $\zeta = 0$. At the critical point $\delta_0^c = \pi/4$, a "0-0" transition occurs from an even-parity singlet state to an even-parity $s_z = -1$ state. There is no spin doublet phase.

$$s_z = -\int_{-L_W}^{L_W} dx\, \frac{\partial_x \phi_s^{(0)}(x)}{2\pi} = 0, \tag{22}$$

$$J = \int_{-L_W}^{L_W} dx\, \frac{\partial_x \theta_c^{(0)}(x)}{\pi} = 0, \tag{23}$$

in agreement with the fact that the BCS ground state has zero total spin and even fermion parity, corresponding to a condensate of Cooper pairs (i.e., a global singlet). The energy of these solutions is obtained replacing the above solutions into Eq. (20)

$$E_0 = \frac{2\Delta}{\pi a} \int_{-L_W}^{L_W} dx \left[\cos\phi_s^{(0)} \cos\theta_c^{(0)} + 1\right] = 0, \tag{24}$$

where we have substracted a uniform background contribution so that these uniform configurations *define* the zero of energy. Quantum corrections computed on top of these solutions give rise to the standard (gapped) superconducting spectrum [41].

(2) *Soliton or kink-type* solutions, corresponding to configurations in which the fields are localized at a particular minimum for $x \to -L_W$ [i.e., $(\phi_s(-L_W), \theta_c(-L_W)) \to (\pi n, \pi m)$] but which develop a discrete "kink" to a neighboring minimum at some point along the x axis. These configurations naturally have higher energy, and we will discuss them in better detail in the following sections (limit $\delta_0 \to 0$ in Figs. 2 and 3). The kink can occur either:

(a) Only in the field ϕ_s. In this case, a jump of size $\pm 2\pi$ occurs in ϕ_s while the other field θ_c remains unaffected, and the corresponding kink connects the minima $(\pi n, \pi m) \to (\pi(n \pm 2), \pi m)$. From Eqs. (17) and (18), the quantum numbers associated to this solution are $s_z = \mp 1$ and $J = 0$, and we conclude that these are solutions with even fermion parity and spin 1.

(b) Simultaneously in *both fields*: the kink connects the minima $(\pi n, \pi m) \to (\pi(n \pm 1), \pi(m \pm 1))$. These kinks imply that $s_z = \mp\frac{1}{2}$ and $J = \pm 1$, and therefore they represent

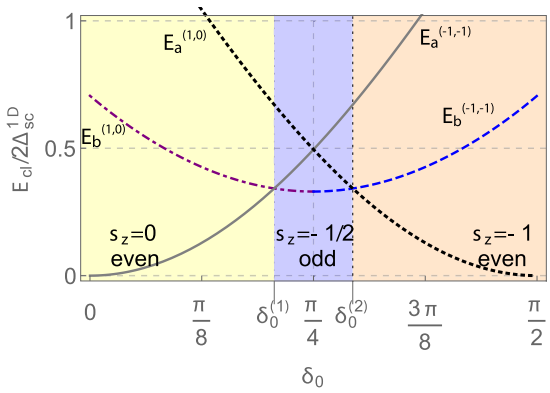

FIG. 3. Energies of the different kink configurations for the interacting 1D system and for $\zeta = -0.4$. At $\delta_0 = \delta_0^{(1)}(\delta_0^{(2)})$ the system exhibits a phase transition from an even-parity singlet state to an odd-parity spin-1/2 doublet (odd-parity spin-1/2 doublet to an even-parity triplet).

solutions where the ground state has odd fermion parity and spin 1/2.

(c) Only in the field θ_c. In this case, the corresponding kink connects the degenerate minima $(\pi n, \pi m) \to (\pi n, \pi(m \pm 2))$. The associated quantum numbers are $s_z = 0$ and $J = \pm 2$, meaning that these are spin 0 solutions with even fermion parity.

B. Solutions at the helical point

At the so-called "helical point" $\zeta = 0$, analytical solutions of Eqs. (17) and (18) can be obtained. To motivate this discussion, we can define the new fields

$$\phi_\pm = \tfrac{1}{2}(\phi_s \pm \theta_c), \tag{25}$$

$$\theta_\pm = \tfrac{1}{2}(\theta_s \pm \phi_c), \tag{26}$$

in terms of which the Hamiltonian terms in Eqs. (6), (8), and (10) become

$$H_0 = \int_{-L_W}^{L_W} dx \left\{ \frac{K_\phi v_\phi}{4\pi} \sum_{\mu=\pm} (\partial_x \phi_\mu)^2 + 2\zeta \partial_x \phi_+ \partial_x \phi_- + \frac{K_\theta v_\theta}{4\pi} \left[\sum_{\mu=\pm} (\partial_x \theta_\mu)^2 + 2\lambda \partial_x \theta_+ \partial_x \theta_- \right] \right\}, \tag{27}$$

$$H_\Delta^{1D} = \frac{\Delta}{\pi a} \int_{-L_W}^{L_W} dx \, [\cos 2\phi_+ + \cos 2\phi_-], \tag{28}$$

$$H_M^{1D} = -\frac{2 v_s \delta_0}{\pi K_s} [\partial_x \phi_+(0) + \partial_x \phi_-(0)], \tag{29}$$

where we have defined the quantities $K_\theta v_\theta = (v_c/K_c + v_s K_s)$, $K_\phi v_\phi = (v_s/K_s + K_c v_c)$, and the parameter

$$\lambda \equiv \frac{(v_c/K_c - v_s K_s)}{(v_c/K_c + v_s K_s)}, \tag{30}$$

which, since it is associated to the canonical momenta $\partial_x \theta_\mu / \pi$, will not appear at the level of the *static* equations of motion and therefore will be ignored in the following.

Note that when $\zeta = 0$, Eqs. (17) and (18) decouple and become

$$\partial_x^2 \phi_\mu = -\frac{g}{2} \sin 2\phi_\mu + 2\delta_0 \delta'(x). \quad (\mu = \pm) \tag{31}$$

This decoupling of fields $\phi_+(x)$ and $\phi_-(x)$ is also evident in Eqs. (27)–(29). In addition, note that in the absence of impurity, $\delta_0 \to 0$ and Eq. (31) takes the form of the celebrated sine-Gordon equation, whose solutions are very well known [41].

To solve Eq. (31) for a generic δ_0, we express the fields $\phi_\pm(x)$ as

$$\phi_\mu(x) = \eta_\mu \frac{\pi}{2} + 2\delta_0 \Theta(x) + \varphi_\mu(x) \quad (\mu = \pm), \tag{32}$$

where the unit-step function $\Theta(x)$ allows us to eliminate the term $\delta'(x)$ in (31) and where $\varphi_\mu(x)$ is a continuous and smooth function at $x = 0$. Note that the composite solitonlike functions

$$\varphi_\mu = \begin{cases} 2 \arctan e^{\eta_\mu \sqrt{g}(x - x_0)} & \text{for } x < 0, \\ 2 \arctan e^{\eta_\mu \sqrt{g}(x + x_0)} + \pi \eta_\mu l_\mu - 2\delta_0 & \text{for } x \geqslant 0, \end{cases} \tag{33}$$

are *exact solutions* of Eq. (31) (see also Appendix A). This is one of the central results of our work. Here, $\eta_\mu = \pm 1$ is an integer which determines the nature of the solution: either soliton ($\eta_\mu = +1$) or antisoliton ($\eta_\mu = -1$). In addition, the integer $l_\mu = 0, \pm 1, \pm 2, \ldots$ determines the different minima of the $\cos 2\phi_\mu$ potential in Eq. (28). Finally, x_0 is a parameter which must be chosen so that the continuity condition at the origin $\varphi_\mu(0^-) = \varphi_\mu(0^+)$ is verified. From this condition we obtain the equation

$$\arctan[\sinh(\eta_\mu \sqrt{g} x_0)] = \delta_0 - \eta_\mu l_\mu \frac{\pi}{2}, \tag{34}$$

from where x_0 is obtained. Once the value of δ_0 and η_μ are fixed, the integer l_μ becomes restricted to only two possibilities since the left hand side of Eq. (34) can only vary between $-\pi/2$ and $\pi/2$.

Of special importance here is the physical meaning associated with the topological charge of the solitonlike solutions (32) and (33). Replacing them into Eqs. (12) and (13), we obtain

$$s_z = -\frac{1}{2} \sum_{\mu=\pm} \eta_\mu (l_\mu + 1), \tag{35}$$

$$J = \sum_{\mu=\pm} (\mu) \eta_\mu (l_\mu + 1). \tag{36}$$

In addition, replacing them into the expression of the classical energy Eq. (20) allows us to obtain

$$E(\delta_0) = \sum_{\mu=\pm} E_\mu^{(\eta_\mu, l_\mu)}(\delta_0), \tag{37}$$

where

$$E_{\mu}^{(\eta_\mu,l_\mu)}(\delta_0) = \frac{v_s}{2\pi K_s}\int_{-L_W}^{L_W} dx\Big[(\partial_x\phi_\mu - 2\delta_0\delta(x))^2 + \frac{g}{2}(\cos 2\phi_\mu + 1)\Big], \quad (38)$$

where we have substracted the constant background term, as in Eq. (24), so that the ground-state energy for $\delta_0 = 0$ (i.e., decoupled impurity) is zero.

Therefore, the integers η_μ and l_μ determine the topological quantum numbers s_z and J in the ground state and refer to a particular "energy branch" $E_{\mu}^{(\eta_\mu,l_\mu)}(\delta_0)$ associated to those quantum numbers (see Fig. 2). Interestingly, in the limit $L_W \to \infty$ the function $E_{\mu}^{(\eta_\mu,l_\mu)}(\delta_0)$ has a simple analytical expression

$$\frac{E_{\mu}^{(\eta_\mu,l_\mu)}(\delta_0)}{2\Delta_{\rm sc}} = 1 - \text{sign}(x_0)\left|\sin\left(\delta_0 - \frac{\pi\eta_\mu l_\mu}{2}\right)\right|, \quad (39)$$

where we have defined $\Delta_{\rm sc} \equiv \frac{v_s\sqrt{g}}{\pi K_s}$.

With the knowledge of these solutions, we can now return to the original fields $\phi_s(x)$ and $\theta_c(x)$ through the relations (25) and (26). Note that since Eq. (31) is identical for ϕ_+ and ϕ_-, it is easy to see that these solutions must be degenerate. Then, at the helical point $\zeta = 0$, the classical ground-state configurations for the original fields are

$$\phi_s(x) = \phi_+(x) + \phi_-(x) = 4\delta_0\Theta(x) + \varphi_+(x) + \varphi_-(x), \quad (40)$$

$$\theta_c(x) = \phi_+(x) - \phi_-(x) = 0, \quad (41)$$

i.e., while $\phi_s(x)$ strongly depends on the value of δ_0; at the helical point $\zeta = 0$ the field $\theta_c(x)$ is fixed to one of the trivial configurations (i.e., $\theta_c^{(0)} = 0$) and remains unaffected by the impurity.

In Fig. 2 we show the three lowest energy branches of the system as functions of the phase shift δ_0 at the helical point $\zeta = 0$. The total ground-state energy is given by the sum of the lowest degenerate branches at a particular value of δ_0. For $\delta_0 < \pi/4$, the ground-state energy is given by $E_{\rm GS}(\delta_0) = \sum_\mu E_\mu^{(-1,-1)}(\delta_0)$ and corresponds to an even-parity singlet phase with topological numbers $s_z = 0$ and $J = 0$ (see blue line in Fig. 2). On the other hand, for $\delta_0 > \pi/4$ the ground state switches to a magnetic branch (topological number $s_z = -1$), with even fermion-parity ($J = 2$), and its energy is $E_{\rm GS}(\delta_0) = \sum_\mu E_\mu^{(+1,0)}(\delta_0)$ (black dashed line). The value $\delta_0^{\rm c} = \pi/4$ indicates a critical point at which the ground-state branches cross. This constitutes a transition that *preserves parity but not the spin*, in stark contrast to the known case in 3D (see Sec. V), and for that reason we dubbed it "0-0" transition. This result can be understood due to the presence of *two* independent bosonic modes $\phi_\pm(x)$ in a 1D geometry. Physically, these modes are related to the fermionic bilinears $\cos 2\phi_+ \sim \psi_{R\uparrow}^\dagger\psi_{L\downarrow}^\dagger$ and $\cos 2\phi_- \sim \psi_{L\uparrow}^\dagger\psi_{R\downarrow}^\dagger$, each one capable of binding independently one Shiba state with $s_z = -1/2$ at the critical point. Therefore, this transition occurs when these two Shiba states simultaneously cross the Fermi energy and become occupied. Thus, the spin quantum number of the ground state jumps from $s_z = 0$ to $s_z = -1$, whereas the ground-state parity remains unchanged. Note that for this transition to be observed it is crucial to avoid the mixing of the fields $\phi_\pm(x)$, something that requires that the magnetization profile induced by the FMI nanowire in Fig. 1 is sufficiently smooth and extended as compared to the scale of $k_{\rm F}^{-1}$, in order for the single-particle backwards scattering terms $\sim e^{i2k_{\rm F}x}e^{i\phi_c(x)}$ are suppressed.

Finally, it is interesting to explore the effect of the experimental details on the 0-0 transition at the helical point. In particular, from Eq. (11) it is easy to see that the critical point $\delta_0^{\rm c} = \pi/4$ is obtained for

$$Vm_0d\sqrt{\pi} = \frac{4v_s}{K_s}. \quad (42)$$

In other words, the critical point can be *tuned* either by injecting spin currents in the FMI nanowire, which would have the effect of modulating the induced exchange field V through spin transfer torques [42,43], or by changing the width d of the FMI nanowire. In addition, note that the critical point also *depends on the interactions* through the parameters v_s and K_s. We stress that this effect is unique of the 1D geometry and has no analog in the 3D case.

C. Approximate results for finite ζ

In this Section, we provide approximate results at finite helicity ζ. As mentioned before, finding analytical solutions for the generic case of Eqs. (17) and (18) is a hard task. Intuitively, a finite ζ results in a highly nontrivial coupling of the fields ϕ_+ and ϕ_-, as is evident from Eq. (27). Therefore, we return to the equations of motion (17) and (18) in terms of the fields ϕ_s and θ_c. In Sec. IV A we discussed topologically nontrivial solutions in the case of a clean superconductor (i.e., $\delta_0 = 0$), which were classified according to their topological quantum numbers s_z and J (cases *a*, *b*, *c* in Sec. IV A). Here, we will construct approximate *ansätze* that describe the correct physical behavior of the fields in the case of a finite δ_0, built upon cases *a*, *b*, and *c* when $\delta_0 = 0$.

Note that generically $\theta_c(x)$ is a smooth and continuous function at $x = 0$, and therefore should satisfy the boundary conditions $\theta_c(0^-) = \theta_c(0^+)$ and $\partial_x\theta_c(0^-) = \partial_x\theta_c(0^+)$. On the other hand, the field $\phi_s(x)$ must satisfy the conditions (see Appendix A)

$$\phi_s(0^+) - \phi_s(0^-) = 4\delta_0, \quad (43)$$

$$\partial_x\phi_s(0^+) - \partial_x\phi_s(0^-) = 0. \quad (44)$$

For a finite δ_0, it is easy to see that solutions of type (c) are not compatible with these boundary conditions, since a constant $\phi_s(x)$ is inconsistent with Eq. (43), and must be excluded from the possible anstäze. We therefore seek for approximate solutions $(\phi_s^{(j)}, \theta_c^{(j)})$, where j refers to the cases $j = a$ or b in Sec. IV A. We also define

$$\phi_s^{(j)}(x) = 4\delta_0\Theta(x) + \varphi_s^{(j)}(x), \quad (45)$$

where $\varphi_s^{(j)}(x)$ is a smooth function with continuous derivative at $x = 0$. Using the results of Ref. [44], we propose the

following approximate solutions

$$\theta_c^{(a)}(x) = n\pi, \tag{46}$$

$$\varphi_s^{(a)}(x) = m\pi + \begin{cases} 4\arctan e^{\eta_s\sqrt{\frac{g}{1-\zeta}}(x-x_0^{(a)})} + (\eta_s - 1)\pi & \text{for } x < 0, \\ 4\arctan e^{\eta_s\sqrt{\frac{g}{1-\zeta}}(x+x_0^{(a)})} + (\eta_s - 1)\pi + \eta_s 2\pi l - 4\delta_0 & \text{for } x > 0, \end{cases} \tag{47}$$

and

$$\theta_c^{(b)}(x) = n\pi + 2\arctan e^{\eta_c\sqrt{\frac{g}{1+\zeta}}x} + \frac{\eta_c - 1}{2}\pi, \tag{48}$$

$$\varphi_s^{(b)}(x) = m\pi + \begin{cases} 2\arctan e^{\eta_s\sqrt{\frac{g}{1-\zeta}}(x-x_0^{(b)})} + \frac{\eta_s-1}{2}\pi & \text{for } x < 0, \\ 2\arctan e^{\eta_s\sqrt{\frac{g}{1-\zeta}}(x+x_0^{(b)})} + \frac{\eta_s-1}{2}\pi + \eta_s 2\pi l - 4\delta_0 & \text{for } x > 0, \end{cases} \tag{49}$$

with (n, m)=(even, odd) or (odd, even). Similarly to the previous Eq. (33), here η_s corresponds to $\eta_{s(c)} = +1$ for the solitonlike solution, and $\eta_{s(c)} = -1$ to the antisolitonlike solution. In addition, the integer $l = 0, \pm 1, \pm 2, \ldots$ determines the specific minima of the $\sim\cos\phi_s(x)$ potential in Eq. (8). For simplicity, the solutions (46)–(49) have been chosen to converge to the same minimum of H_Δ^{1D} in Eq. (8), i.e., $(\phi_s^{(j)}(x), \theta_c^{(j)}(x)) \xrightarrow[x\to-\infty]{} (m\pi, n\pi)$. Imposing the continuity condition for $\varphi_s^{(j)}(x)$ and its derivative at $x = 0$, we obtain the equation:

$$\arctan\left[\sinh\left(\eta_s\sqrt{\frac{g}{1-\zeta}}x_0^{(j)}\right)\right] = A_j\left(\delta_0 - \frac{\eta_s l\pi}{2}\right), \tag{50}$$

which determines the parameter $x_0^{(j)}$ (here we have defined $A_a = 1$ and $A_b = 2$). Once Eq. (50) is solved for given values of δ_0, η_s, l and the helicity ζ, the solution $(\phi_s^{(j)}, \theta_c^{(j)})$ is completely determined. Replacing it into Eqs. (12) and (13), we obtain the topological quantum numbers s_z and J:

$$s_z^{(a)} = \eta_s(1 + l), \quad J^{(a)} = 0, \tag{51}$$

$$s_z^{(b)} = \eta_s\left(\tfrac{1}{2} + l\right), \quad J^{(b)} = \eta_c. \tag{52}$$

Note that the solutions of type $a(b)$ correspond to a ground state with integer (semi-integer) spin s_z. In addition, replacing the solution $(\phi_s^{(j)}, \theta_c^{(j)})$ into Eq. (16) and integrating, we obtain (up to a constant contribution):

$$E_a^{(\eta_s,l)}(\delta_0) = \frac{v_s}{4\pi K_s} 16\sqrt{\frac{g}{1-\zeta}}\left[1 - \text{sign}\left(x_0^{(a)}\right)\left|\sin\left(\delta_0 - \frac{\pi\eta_s l}{2}\right)\right|\right], \tag{53}$$

$$E_b^{(\eta_s,l)}(\delta_0) = \frac{v_s}{4\pi K_s} 2\sqrt{\frac{g}{1-\zeta}}\left[1 - \text{sign}\left(x_0^{(b)}\right)|\sin(2\delta_0 - \pi\eta_s l)| + \sqrt{\frac{1+\zeta}{1-\zeta}} + 2F\left(\sqrt{\frac{g}{1-\zeta}}x_0^{(b)}, \zeta\right)\right], \tag{54}$$

where we have defined the dimensionless function

$$F(y_0, \zeta) \equiv \int_0^\infty dy\left[1 - \tanh\left(\sqrt{\frac{1-\zeta}{1+\zeta}}y\right)\tanh(y + y_0)\right]. \tag{55}$$

In order to compare with the usual superconductor gap in the spectrum of fermionic quasiparticles, here we define the single-particle energy gap in the clean case ($\delta_0 = 0$) as the difference between the lowest spin-0 energy branch and the first spin-1/2 energy branch. Explicitly in our case, this corresponds to the formula:

$$2\Delta_{SC}^{1D} = E_b^{(+1,0)}(0) - E_a^{(-1,-1)}(0) = \frac{2v_s\sqrt{g}}{\pi K_s}, \tag{56}$$

where we have assumed the helical condition $\zeta = 0$ in order to appreciate the deviations from helicity in Fig. 2.

The results in this section are summarized in Fig. 3, obtained for the particular value $\zeta = -0.4$. The most important feature in this figure, as compared to Fig. 2, is the splitting of the 0-0 transition into two 0-π transitions occurring at the critical points $\delta_0^{(1)} = 0.65$ and $\delta_0^{(2)} = 0.92$. This splitting is concomitant of an intermediate phase with spin $s_z = -1/2$ and odd fermion parity (see light blue region in Fig. 3) which emerges in between the $s_z = 0$ and $s_z = -1$ even parity phases. The new critical points $\delta_0^{(1)}$ and $\delta_0^{(2)}$ appear, respectively, from the crossing of the branches $E_a^{(-1,-1)}$ and $E_b^{(+1,0)}$, and $E_b^{(-1,-1)}$ and $E_a^{(+1,0)}$. The new phase appears due to the stabilization of the odd-parity $s_z = -1/2$ energy branches, with respect to the $\zeta = 0$ case, a fact that can be physically understood because for $\zeta < 0$ the deformations of the field ϕ_s become energetically less costly than the deformations of θ_c.

V. BOSONIZATION OF A SHIBA IMPURITY IN A 3D SUPERCONDUCTOR

Although our work mainly deals with a 1DNW, it is illuminating to briefly turn to the well-known case of a magnetic impurity in a 3D superconductor [1–3]. Interestingly, within the Abelian bosonization formalism this problem can be considered as a *particular case* of the 1D geometry studied before. Indeed, for a pointlike magnetic impurity placed at the origin of a 3D superconductor (described by a spherically symmetric BCS model), only the s-wave component $\Psi_\sigma^s(\boldsymbol{r})$ of the 3D Fermi field couples to the impurity. Then, linearizing the spectrum around the Fermi energy, we can write [30]

$$\Psi_\sigma^s(\boldsymbol{r}) = \frac{1}{i2\sqrt{\pi}r}[e^{ik_F r}\psi_{L\sigma}(r) - e^{-ik_F r}\psi_{R\sigma}(r)], \tag{57}$$

where $0 \leqslant r \leqslant \infty$ is the radial coordinate. Equivalently, the half line can be unfolded to the whole axis by defining

$$\psi_{r,\sigma}(-x) \equiv \psi_{-r,\sigma}(x), \quad (r = L, R) \tag{58}$$

and keeping a *single chirality* for each fermion. This definition includes the boundary condition $\psi_{R\sigma}(0) = \psi_{L\sigma}(0)$ at $x = 0$, which guarantees that $\Psi^{\rm s}_\sigma(x)$ is finite at the origin. This procedure is standard and we refer the reader to Refs. [29,30] for details. In what follows, when treating the 3D case, we will keep only the branches $\psi_{L\uparrow}$ and $\psi_{R\downarrow}$. Imposing a hard-wall boundary condition in a sphere of radius R (i.e., $\Psi^{\rm s}_\sigma(R) = 0$) induces periodic boundary conditions on the effective 1D chiral fermions, $\psi_{r\sigma}(-R) = \psi_{r\sigma}(R)$. Therefore, we can write $H^{\rm 3D}_0 = -iv_F \int_{-R}^{R} dx\,[\psi^\dagger_{R\downarrow}\partial_x\psi_{R\downarrow} - \psi^\dagger_{L\uparrow}\partial_x\psi_{L\uparrow}]$. Interestingly, this is the same Hamiltonian that describes the edge states of a spin-Hall insulator [45]. Upon bosonization, this Hamiltonian becomes

$$H^{\rm 3D}_0 = \frac{v_F}{2\pi}\int_{-R}^{R} dx\,[(\partial_x\phi_-(x))^2 + (\partial_x\theta_-(x))^2], \tag{59}$$

where *only the field* $\phi_-(x)$ *appears*. In addition, since the (repulsive) interactions are efficiently screened in a 3D superconductor, we have $K_c = K_s = 1$ and $v_s = v_c = v_F$, and the system is automatically at the helical point $\zeta = 0$ seen in Sec. IV B. On the other hand, it is easy to see that due to the elimination of the chiral fields $\psi_{R\uparrow}$ and $\psi_{L\downarrow}$, the pairing Hamiltonian in the s-wave channel writes

$$\begin{aligned} H^{\rm 3D}_\Delta &= \Delta\int_{-R}^{R} dx\,[\psi^\dagger_{L\uparrow}(x)\psi^\dagger_{R\downarrow}(x) + \text{H.c.}], \\ &= \frac{\Delta}{\pi a}\int_{-R}^{R} dx\,\cos 2\phi_-(x), \end{aligned} \tag{60}$$

where here Δ is the intrinsic (i.e., originated in the electron-phonon interaction) pairing interaction.

Finally, the presence of a classical spin is usually modelled using the s-d Hamiltonian [1–3]: $H^{\rm 3D}_M = \frac{JS^z}{2}[\Psi^{\rm s\dagger}_\uparrow(0)\Psi^{\rm s}_\uparrow(0) - \Psi^{\rm s\dagger}_\downarrow(0)\Psi^{\rm s}_\downarrow(0)]$, where J is the s-d exchange coupling and $S^z = \pm S$ is the z component of the magnetic impurity S, assumed as an Ising spin. In terms of the chiral fields, this term writes $H^{\rm 3D}_M = \frac{Jk_F^2 S^z}{2\pi}[\psi^\dagger_{L\uparrow}(0)\psi_{L\uparrow}(0) - \psi^\dagger_{R\downarrow}(0)\psi_{R\downarrow}(0)]$, where we have used Eq. (58) and the result $\lim_{r\to 0}\Psi^{\rm s}_\sigma(\boldsymbol{r}) = \frac{k_F}{2\sqrt{\pi}}[\psi_{L\sigma}(0) + \psi_{R\sigma}(0)]$. Again, $H^{\rm 3D}_M$ can be absorbed via the gauge transformation $\psi_{L\uparrow(R\downarrow)}(x) \to \tilde\psi_{L\uparrow(R\downarrow)}(x) = e^{\mp i2\delta^{\rm 3D}_0\Theta(x)}\psi_{L\uparrow(R\downarrow)}(x)$, where

$$\delta^{\rm 3D}_0 = \arctan\left(\frac{JS^z\rho_0\pi}{2}\right) \tag{61}$$

is the s-wave phase shift (note that we have used the definition of the density of states at the Fermi level $\rho_0 = k_F^2/4\pi v_F$) [4]. Then, in bosonic language we obtain the expression

$$H^{\rm 3D}_M = -\frac{2v_F\delta^{\rm 3D}_0}{\pi}\partial_x\phi_-(0). \tag{62}$$

In this way, the connection between $H^{\rm 1D}$ and $H^{\rm 3D}$ can be clearly seen: The 3D Hamiltonian is identical to the 1D Hamiltonian at the point $\zeta = 0$ with *half the degrees of freedom* (i.e., the field $\phi_+(x)$ is absent, and the system becomes a *helical liquid* [45]). Consequently, the classical configuration of the field $\phi_-(x)$ is also given by Eq. (31).

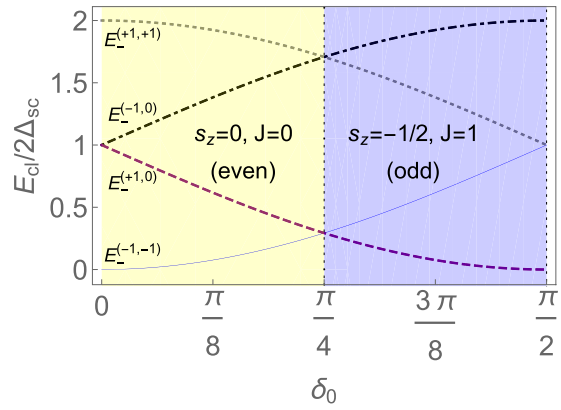

FIG. 4. Phase diagram of the Shiba impurity in 3D: energy of the different branches as a function of the phase shift δ_0 [see Eq. (39)]. At the critical value $\delta_0^{\rm 3D,c} = \pi/4$ the system exhibits a phase transition from an even-parity singlet state to an odd-parity spin-1/2 doublet.

For a decoupled impurity (i.e., when $\delta_0 = 0$), the ground-state configuration of the superconductor is described by a constant $\phi_-(x) = \frac{\pi}{2}$, which trivially minimizes the pairing term $\cos 2\phi_-(x)$ in Eq. (60). This situation physically corresponds to the "classical" BCS ground state. Our solutions (32) and (33) precisely recover this behavior for (η_-, l_-)=$(-1, -1)$, for which Eq. (34) yields $x_0 \to \infty$, and Eq. (39) yields the energy $E_-^{(-1,-1)}(0) = 0$ (see continuous blue line in Fig. 4). This ground state has topological numbers $s_z = 0$ and $J = 0$ (i.e., even-parity singlet), as expected physically for a BCS superconductor. On the other hand, the solution with $\eta_- = +1$ ($\eta_- = -1$) and $l_- = 0$ corresponds to a topological kink (antikink) connecting the minima $\phi_- = \frac{\pi}{2}$ at $x = -\infty$ and $\phi_- = \frac{3\pi}{2}$ ($\phi_- = -\frac{\pi}{2}$) at $x = \infty$, and corresponds to an excited state with $s_z = -1/2$ ($s_z = 1/2$) and $J = -1$ ($J = 1$) (odd-parity doublet). We interpret this state as having an extra (one less) fermion with respect to the BCS ground state and has energy $E_-^{(\pm1,0)}(0) = 2\Delta_{\rm sc}$ (dashed purple line in Fig. 4). Other excited branches are shown in that figure. As the value of δ_0 is increased, the branches $E_-^{(-1,-1)}$ and $E_-^{(\pm1,0)}$ approach each other and eventually cross at the value $\delta_0^{\rm 3D,c} = \pi/4$, signaling a quantum phase transition. This is *precisely* the 0-π transition obtained originally in Refs. [1–3], at which the ground state abruptly changes spin and parity. Interestingly, our formalism allows us to *exactly* recover the critical value of the transition obtained from the crossing of Shiba levels at zero energy [2,4]

$$E_{\rm Shiba} = \pm\frac{1-\alpha^2}{1+\alpha^2}, \tag{63}$$

(where $\alpha = J\rho_0\pi S^z/2$). From here, note that the condition $E_{\rm Shiba} = 0$ precisely corresponds to $\delta_0^{\rm 3D,c} = \pi/4$. In addition to allowing a simple and elegant rederivation of well-known results, the results presented in this section serve as a sanity check for the Abelian bosonization method in this context.

VI. SUMMARY AND CONCLUSIONS

We have studied the ground-state properties and the quantum phase diagram of a classical Shiba impurity in an interacting one-dimensional superconducting nanowire from the perspective of the Abelian bosonization technique. Quantum 1D systems are qualitatively different from their higher-dimensional counterparts, and in the present work we have shown that the quantum phase diagram of a Shiba impurity in a 1D geometry is strongly modified with respect to the usual 0-π transition expected for bulk superconductors with quantum dots or atomic impurities. In addition, we have considered the effect of strong correlations on the ground-state properties of the nanowire, something that is very hard to account for using other analytical approaches.

For concreteness, we have focused the analysis on a hybrid heterostructure consisting of a 1D semiconductor nanowire (1DNW) proximitized by a bulk superconductor which acts as a source of Cooper pairs, similar to those recently fabricated and studied in the context of Majorana experiments [25,26]. The effect of an "artificial" magnetic impurity was considered by assuming the presence of a ferromagnetic insulator (FMI) nanowire inducing a localized exchange field on a scale $d \ll \xi_{1D}$. Under such conditions, the exchange field acts as an artificial "pointlike" magnetic impurity inducing subgap Shiba states, which can be controlled varying the magnetization m_z in the FMI nanowire with, e.g., external magnetic fields or spin-polarized currents.

In particular, as a function of the induced phase shift δ_0, in the helical case $\zeta = 0$ we have found a *parity-preserving* "0-0" transition in which the spin of the ground state changes from $s_z = 0$ to $s_z = \pm 1$. In the more usual quasiparticle-state picture, this transition can be interpreted in terms of two exactly degenerate subgap Shiba states (each hosting a spin-1/2 Bogoliubov quasiparticle) which become simultaneously occupied when they cross the Fermi level.

Although the helical point condition ($\zeta = 0$) studied here is a useful theoretical approximation, it is certainly a highly idealized situation in experiments and it is interesting to analyze possible deviations from it. We have studied the case $\zeta \neq 0$, which has the effect of mixing and splitting the above-mentioned degenerate states, and therefore an intermediate phase where the ground state has spin 1/2 appears (see Fig. 3). In addition, backscattering processes originated by the impurity (i.e., scattering processes with momentum transfer $\Delta q \simeq 2k_F$ occurring between the R and L fermion branches), which have been neglected in this work due to the condition $d \gg k_F^{-1}$, can be considered as another type of experimental "nonideality." Although it is technically very complicated to address in detail these processes within our approach, based on the intuitive picture provided by the noninteracting fermionic picture, we expect that they will have a similar effect to a finite helicity, since they mix right and left movers $\psi_{R\sigma}$ and $\psi_{L\sigma}$, and therefore they can also lift the above-mentioned degeneracy at the helical point. A more detailed study of these effects will be provided in forthcoming works [46].

As mentioned above, the proposed device depicted in Fig. 1 is qualitatively different from the usual superconductor-quantum dot devices and is actually reminiscent of already existing experimental setups fabricated to observe fractionalization of charges in Luttinger liquids [47]. In those experiments, in order to inject electrons with well-defined energy and momentum into a 1D nanowire, it was crucial that the length on the injection contact L_S was $L_S \gg k_F^{-1}$ to avoid momentum transfer processes [47,48]. Although in our case the FMI nanowire *does not* inject electrons into the 1DNW (it is an insulator), it shares the property that single-particle backscattering processes are suppressed. Therefore, we believe that the experimental requirements to fabricate the device proposed in this work can be met using the nowadays available experimental growth techniques. The typical experimental values of $k_F^{-1} \sim 20$ nm found in semiconducting nanowires [49], and the coherence length $\xi_{1D} \approx 260$ nm in proximitized nanowires [50] are encouraging in this respect.

ACKNOWLEDGMENTS

The authors acknowledge support from ANPCyT, PICT 2017-2081, Argentina. A.M.L. acknowledges support from PIP-11220150100364 (CONICET - Argentina) and Relocation Grant No. RD1158 - 52368 (CONICET - Argentina). A.I. gratefully acknowledges support from the Fulbright Foundation and the Hospitality of the University of Maryland where part of this work was completed.

APPENDIX A: SOLUTION OF THE STATIC DEFECTIVE SINE-GORDON EQUATION

Consider the static equation

$$\partial_x^2 \phi(x) = -h \sin \phi(x) + \lambda \partial_x \delta(x). \tag{A1}$$

We shall look for solutions of this equation that satisfy the boundary conditions at infinity

$$\partial_x \phi(\pm\infty) = 0, \tag{A2}$$

$$\sin(\phi(\pm\infty)) = 0, \tag{A3}$$

and that have *at most* a finite discontinuity at the origin. These conditions ensure that solutions are localized in space and that their classical energy is finite [41].

Note that in order to account for the presence of the term $\lambda \partial_x \delta(x)$, the field $\phi(x)$ must allow for extra degrees of freedom as compared to the kink solution. These extra degrees of freedom must be fixed with new conditions at $x = 0$. To obtain these conditions, we first perform the indefinite integral of (A1)

$$\partial_x \phi(x) = -h \int^x dx' \, \sin \phi(x') + \lambda \delta(x) + \text{const.} \tag{A4}$$

If, as stated previously, $\phi(x)$ has at most a finite jump at $x = 0$, then its primitive must be continuous there. Therefore, taking the limit around the origin we obtain the condition to be obeyed by the first derivative

$$\partial_x \phi(0^+) = \partial_x \phi(0^-). \tag{A5}$$

Next, we note that $\phi(x)$ itself cannot be continuous, otherwise its second derivative would give rise to at most a function $\delta(x)$ [and not $\partial_x \delta(x)$]. Thus, integrating again around the origin, we

obtain the second condition

$$\phi(0^+) - \phi(0^-) = \lambda. \tag{A6}$$

This equation is perfectly compatible with (A5), which only fixes $\partial_x\phi$ outside of the origin.

Conditions (A5) and (A6) can be taken into account with the change of variables

$$\phi(x) = \lambda\Theta(x) + \varphi(x), \tag{A7}$$

where $\Theta(x)$ is the unit-step function and $\varphi(x)$ is a continuous function with continuous derivatives. In terms of these new variables, the term $\lambda\partial_x\delta(x)$ is eliminated from Eq. (A1), and we obtain

$$\partial_x^2\varphi(x) = -h\sin[\varphi(x) + \lambda\Theta(x)]. \tag{A8}$$

The solutions of this equation, which are compatible with the conditions (A5) and (A6) can be written as:

$$\varphi_{\eta,n}(x) = \begin{cases} 4\arctan e^{\eta\sqrt{h}(x-x_0)} + \eta\pi & x < 0, \\ 4\arctan e^{\eta\sqrt{h}(x+x_0)} + \eta\pi + \eta 2\pi n - \lambda & x > 0, \end{cases} \tag{A9}$$

where n is an arbitrary integer and where $\eta = +1(-1)$ represents the kink (antikink) solution. Note that due to the form of the solution, Eq. (A5) is automatically satisfied. In addition, here x_0 is an extra degree of freedom to be determined using the condition Eq. (A6). This condition leads to the equation

$$\arctan\sinh(\eta\sqrt{h}x_0) = \frac{\lambda - 2\pi\eta n}{4}, \tag{A10}$$

The left hand side of this equation takes values in the interval $(-\frac{\pi}{2}, \frac{\pi}{2})$, which puts a restriction on the allowed values of n:

$$\frac{\eta\lambda}{2\pi} - 1 < n < \frac{\eta\lambda}{2\pi} + 1. \tag{A11}$$

Since n is an integer, it can only be equal to the roof or ceiling of $\eta\lambda/2\pi$.

The solutions are qualitatively different for the two allowed values of n. For the roof of $\eta\lambda/2\pi$ x_0 turns out to be positive, and the solution has a single kink (or antikink) character. On the contrary, if n is the ceiling of $\eta\lambda/2\pi$, then $x_0 < 0$ and the solution develops a double kink [51]. To better picture the situation, we plot the kink profile φ as a function of the *incline* variable $\gamma = 2\pi(n+1) - \lambda$, that takes values in $(0, 4\pi)$ and signals the "topological charge" $\gamma = \varphi(\infty) - \varphi(-\infty)$. γ is a real number and therefore φ a fractional soliton [51]. For kinks $\gamma \in (0, 2\pi)$ describes simple kinks, whereas $\gamma \in (2\pi, 4\pi)$ is for double kinks. The kink profiles are depicted in Fig. 5. In double kinks, the kink separation behaves as $-x_0 \sim \log(\frac{\gamma}{4} - \pi)$ close to $\gamma = 4\pi$, thus it increases very slowly and must be close to 4π to become appreciable.

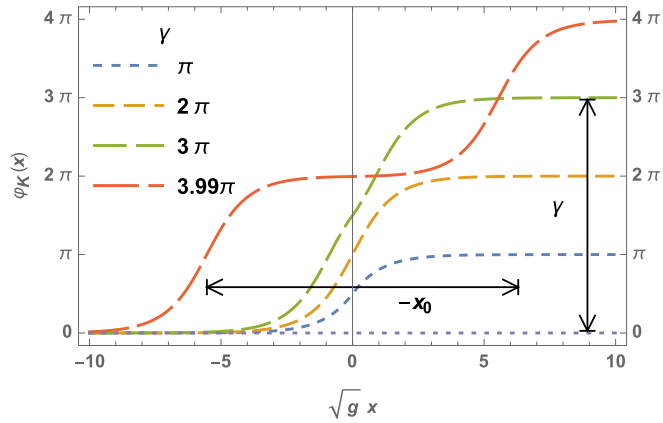

FIG. 5. Shape of the kinks for different values of γ. Notice that at $\gamma = 2\pi$ the shape changes from 1-kink to 2-kinks configuration. γ is equal to the topological charge $\gamma = \varphi_K(\infty) - \varphi_K(-\infty)$.

The energy of this excitation is

$$E = 16\sqrt{h}\sin^2\frac{\gamma}{8}, \tag{A12}$$

and its topological charge (or spin) is obtained from Eq. (5)

$$Q_{\eta,n} = -\frac{1}{2\pi}\int_{-\infty}^{\infty} dx\,\partial_x\phi_{\eta,n}. \tag{A13}$$

Inserting the decomposition of Eq. (A7) we obtain

$$Q_{\eta,n} = -\frac{\lambda}{2\pi} - \frac{\varphi_{\eta,n}(+\infty) - \varphi_{\eta,n}(-\infty)}{2\pi} = -\eta(n+1). \tag{A14}$$

Notice that there is a cancellation of the contribution from the origin and the total topological charge takes an integer value.

[1] L. Yu, Acta Phys. Sin. **21**, 75 (1965).
[2] H. Shiba, Prog. Theor. Phys. **40**, 435 (1968).
[3] A. I. Rusinov, Zh. Eksp. Teor. Fiz. Pisma Red. **9**, 146 (1968) [JETP Lett. **9**, 85 (1969)].
[4] A. V. Balatsky, I. Vekhter, and J.-X. Zhu, Rev. Mod. Phys. **78**, 373 (2006).
[5] S. De Franceschi, L. Kouwenhoven, C. Schönenberger, and W. Wernsdorfer, Nat. Nanotechnol. **5**, 703 (2010).
[6] R. S. Deacon, Y. Tanaka, A. Oiwa, R. Sakano, K. Yoshida, K. Shibata, K. Hirakawa, and S. Tarucha, Phys. Rev. Lett. **104**, 076805 (2010).
[7] A. Martín-Rodero and A. L. Yeyati, Adv. Phys. **60**, 899 (2011).
[8] R. Maurand, T. Meng, E. Bonet, S. Florens, L. Marty, and W. Wernsdorfer, Phys. Rev. X **2**, 011009 (2012).
[9] C. Nayak, S. H. Simon, A. Stern, M. Freedman, and S. Das Sarma, Rev. Mod. Phys. **80**, 1083 (2008).
[10] S. Nadj-Perge, I. K. Drozdov, B. A. Bernevig, and A. Yazdani, Phys. Rev. B **88**, 020407(R) (2013).
[11] J. Klinovaja, P. Stano, A. Yazdani, and D. Loss, Phys. Rev. Lett. **111**, 186805 (2013).
[12] B. Braunecker and P. Simon, Phys. Rev. Lett. **111**, 147202 (2013).
[13] F. Pientka, L. I. Glazman, and F. von Oppen, Phys. Rev. B **88**, 155420 (2013).
[14] A. Y. Kitaev, Phys. Usp. **44**, 131 (2001).
[15] S. Nadj-Perge, I. K. Drozdov, J. Li, H. Chen, S. Jeon, J. Seo, A. H. MacDonald, B. A. Bernevig, and A. Yazdani, Science **346**, 602 (2014).

[16] M. Ruby, F. Pientka, Y. Peng, F. von Oppen, B. W. Heinrich, and K. J. Franke, Phys. Rev. Lett. **115**, 197204 (2015).

[17] R. Pawlak, M. Kisiel, J. Klinovaja, T. Meier, S. Kawai, T. Glatzel, D. Loss, and E. Meyer, npj Quantum Inf. **2**, 16035 (2016).

[18] B. E. Feldman, M. T. Randeria, J. Li, S. Jeon, Y. Xie, Z. Wang, I. K. Drozdov, B. Andrei Bernevig, and A. Yazdani, Nat. Phys. **13**, 286 (2016).

[19] A. Sakurai, Prog. Theor. Phys. **44**, 1472 (1970).

[20] K. J. Franke, G. Schulze, and J. I. Pascual, Science **332**, 940 (2011).

[21] J. Bauer, J. I. Pascual, and K. J. Franke, Phys. Rev. B **87**, 075125 (2013).

[22] E. J. H. Lee, X. Jiang, R. Aguado, G. Katsaros, C. M. Lieber, and S. De Franceschi, Phys. Rev. Lett. **109**, 186802 (2012).

[23] J. Schindele, A. Baumgartner, R. Maurand, M. Weiss, and C. Schönenberger, Phys. Rev. B **89**, 045422 (2014).

[24] J. O. Island, R. Gaudenzi, J. de Bruijckere, E. Burzurí, C. Franco, M. Mas-Torrent, C. Rovira, J. Veciana, T. M. Klapwijk, R. Aguado, and H. S. J. van der Zant, Phys. Rev. Lett. **118**, 117001 (2017).

[25] P. Krogstrup, N. L. B. Ziino, W. Chang, S. M. Albrecht, M. H. Madsen, E. Johnson, J. Nygård, C. M. Marcus, and T. S. Jespersen, Nat. Mater. **14**, 400 (2015).

[26] M. Taupin, E. Mannila, P. Krogstrup, V. F. Maisi, H. Nguyen, S. M. Albrecht, J. Nygård, C. M. Marcus, and J. P. Pekola, Phys. Rev. Appl. **6**, 054017 (2016).

[27] C. L. Kane and M. P. A. Fisher, Phys. Rev. Lett. **68**, 1220 (1992).

[28] C. L. Kane and M. P. A. Fisher, Phys. Rev. B **46**, 15233 (1992).

[29] T. Giamarchi, *Quantum Physics In One Dimension* (Oxford University Press, Oxford, 2004).

[30] A. O. Gogolin, A. A. Nersesyan, and A. M. Tsvelik, *Bosonization and Strongly Correlated Systems* (Cambridge, Cambridge, 1988).

[31] R. M. Lutchyn, J. D. Sau, and S. Das Sarma, Phys. Rev. Lett. **105**, 077001 (2010).

[32] J. D. Sau, S. Tewari, R. M. Lutchyn, T. D. Stanescu, and S. D. Sarma, Phys. Rev. B **82**, 214509 (2010).

[33] Y. Oreg, G. Refael, and F. von Oppen, Phys. Rev. Lett. **105**, 177002 (2010).

[34] S. Takei, B. M. Fregoso, H.-Y. Hui, A. M. Lobos, and S. Das Sarma, Phys. Rev. Lett. **110**, 186803 (2013).

[35] S. Gangadharaiah, B. Braunecker, P. Simon, and D. Loss, Phys. Rev. Lett. **107**, 036801 (2011).

[36] A. M. Lobos, R. M. Lutchyn, and S. Das Sarma, Phys. Rev. Lett. **109**, 146403 (2012).

[37] T.-P. Choy, J. M. Edge, A. R. Akhmerov, and C. W. J. Beenakker, Phys. Rev. B **84**, 195442 (2011).

[38] G. C. Ménard, S. Guissart, C. Brun, R. T. Leriche, M. Trif, F. Debontridder, D. Demaille, D. Roditchev, P. Simon, and T. Cren, Nat. Commun. **8**, 2040 (2017).

[39] In fermion language and in the absence of interactions, the Hamiltonian H_M^{1D} can be written as $H_M^{\mathrm{1D}} \simeq \frac{Vm_0 d\sqrt{\pi}}{2} \sum_{r=L,R} [\psi_{r\uparrow}^\dagger(0)\psi_{r\uparrow}(0) - \psi_{r\downarrow}^\dagger(0)\psi_{r\downarrow}(0)]$. This term can be eliminated via a gauge transformation $\psi_{r\sigma} \to \tilde{\psi}_{r\sigma} = e^{i2r\sigma\delta_0\Theta(x)}\psi_{r\sigma}$, where $\Theta(x)$ is the unit step function.

[40] F. D. M. Haldane, Phys. Rev. Lett. **47**, 1840 (1981).

[41] R. Rajaraman, *Solitons and instantons - An introduction to Solitons and Instantons in Quantum Field Theory* (Elsevier, Amsterdam, 1982).

[42] J. C. Slonczewski, J. Magn. Magn. Mater. **159**, L1 (1996).

[43] L. Berger, Phys. Rev. B **54**, 9353 (1996).

[44] V. M. Krasnov, Phys. Rev. B **85**, 134525 (2012).

[45] C. Wu, B. A. Bernevig, and S.-C. Zhang, Phys. Rev. Lett. **96**, 106401 (2006).

[46] T. Bortolin, A. Iucci, and A. M. Lobos (unpublished).

[47] H. Steinberg, G. Barak, A. Yacoby, L. N. Pfeiffer, K. W. West, B. I. Halperin, and K. Le Hur, Nat. Phys. **4**, 116 EP (2007).

[48] K. Le Hur, B. I. Halperin, and A. Yacoby, Ann. Phys. **323**, 3037 (2008).

[49] T. S. Jespersen, M. L. Polianski, C. B. Sørensen, K. Flensberg, and J. Nygård, New J. Phys. **11**, 113025 (2009).

[50] S. M. Albrecht, A. P. Higginbotham, M. Madsen, F. Kuemmeth, T. S. Jespersen, J. Nygård, P. Krogstrup, and C. M. Marcus, Nature (London) **531**, 206 (2016).

[51] Y.-F. Hsu and J.-J. Su, Sci. Rep. **5**, 15796 (2015).